Biochemistry

Article

pubs.acs.org/biochemistry

Eukaryotic Ribosomal Expansion Segments as Antimicrobial Targets

Lizzette M. Gómez Ramos,[†,‡] Natalya N. Degtyareva,[§] Nicholas A. Kovacs,[†] Stefany Y. Holguin,[‡] Liuwei Jiang,[∥] Anton S. Petrov,[†] Marcin Biesiada,[⊥] Michael Y. Hu,[†] Katarzyna J. Purzycka,[⊥] Dev P. Arya,[§,∥] and Loren Dean Williams*[,†]

[†]School of Chemistry and Biochemistry, Georgia Institute of Technology, 315 Ferst Drive NW, Atlanta, Georgia 30332-0363, United States

[‡]School of Chemical and Biomolecular Engineering, Georgia Institute of Technology, 311 Ferst Drive NW, Atlanta, Georgia 30332-0100, United States

[§]NUBAD, LLC, 900 B West Farris Road, Greenville, South Carolina 29605, United States

[∥]Department of Chemistry, Clemson University, 436 Hunter Laboratories, Clemson, South Carolina 29634-0973, United States

[⊥]RNA Structure and Function Laboratory, Institute of Bioorganic Chemistry, Polish Academy of Sciences, Poznan 61-704, Poland

Supporting Information

ABSTRACT: Diversity in eukaryotic rRNA structure and function offers possibilities of therapeutic targets. Unlike ribosomes of prokaryotes, eukaryotic ribosomes contain species-specific rRNA expansion segments (ESs) with idiosyncratic structures and functions that are essential and specific to some organisms. Here we investigate expansion segment 7 (ES7), one of the largest and most variable expansions of the eukaryotic ribosome. We hypothesize that ES7 of the pathogenic fungi *Candida albicans* ($ES7_{CA}$) could be a prototypic drug target. We show that isolated $ES7_{CA}$ folds reversibly to a native-like state. We developed a fluorescence displacement assay using an RNA binding fluorescent probe, F-neo. F-neo binds tightly to $ES7_{CA}$ with a K_d of 2.5×10^{-9} M but binds weakly to ES7 of humans ($ES7_{HS}$) with a K_d estimated to be greater than 7 μM. The fluorescence displacement assay was used to investigate the affinities of a library of peptidic aminosugar conjugates (PAs) for $ES7_{CA}$. For conjugates with highest affinities for $ES7_{CA}$ (NeoRH, NeoFH, and NeoYH), the lowest dose needed to induce mortality in *C. albicans* (minimum inhibitory concentration, MIC) was determined. PAs with the lowest MIC values were tested for cytotoxicity in HEK293T cells. Molecules with high affinity for $ES7_{CA}$ *in vitro* induce mortality in *C. albicans* but not in HEK293T cells. The results are consistent with the hypothesis that ESs represent useful targets for chemotherapeutics directed against eukaryotic pathogens.

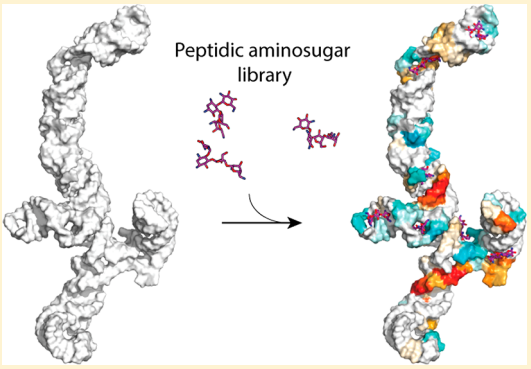

Many antibiotics bind to regions of rRNAs (rRNAs) that are common to all organisms. These universal regions of rRNAs, called the common core,[1,2] contain the A site, the P site, the exit tunnel, the peptidyl transfer center, and the decoding center.[3] These functional centers are targeted by macrolides, aminoglycosides, tetracyclines, streptogramins, pleuromutilins, chloramphenicol, linezolid, and puromycin.[4] Increasing resistance to these antibiotics[5,6] motives a search for new antibiotic targets.[7]

Eukaryotic pathogens, including various fungi, are gaining drug resistance in parallel with bacterial pathogens.[8] Unlike those of prokaryotes, eukaryotic ribosomes contain species-specific rRNA expansions. To our knowledge, eukaryotic rRNA expansion segments (ESs)[2,9−13] are substantially unexplored as drug targets. ESs emerge from the surface of the common core[2] and are characterized by idiosyncratic structures and functions that are essential and specific to various species. ESs are important for ribosome biogenesis,[14,15] rRNA processing and stabilization,[16,17] translation initiation, and recruitment of factors such as chaperones, enzymes, aminoacyl tRNA synthetases, and signal recognition particles.[18−21] Expansion segment 7 (ES7), the largest and most variable ES of the ribosome, is an extension of the ribosomal large subunit (LSU) rRNA.

Here we use ES7 of *Candida albicans* ($ES7_{CA}$) to investigate the general utility of ESs as targets for chemotherapeutic agents and to develop new approaches for eukaryotic drug targeting. *C. albicans*, along with *Cryptococcus neoformans*, *Coccidioides immitis*, and *Pneumocystis jiroveci* affect immunocompromised populations including AIDS and cancer patients, organ-transplant recipients, low-birth-weight infants, and individuals with inherited diseases.[22,23] Candidiasis is the fourth leading cause of healthcare associated blood infections in the United States.[24]

Received: July 22, 2017
Revised: August 29, 2017
Published: September 12, 2017

DOI: 10.1021/acs.biochem.7b00703
Biochemistry 2017, 56, 5288−5299

C. albicans and related species show resistance to antimicrobial agents such as fluconazole.[25,26]

ES7 rRNA of fungi, which is conserved in secondary structure, averages around 210 nucleotides (nts) in length (Table S.3, Figure S.1). $ES7_{CA}$ is 209 nts with ~55% GC content (*C. neoformans*, 234 nts, ~ 50% GC; *C. immitis*, 210 nts, ~ 60% GC; *P. jiroveci*, 223 nts, ~ 50% GC). By contrast, ES7 of *Homo sapiens* ($ES7_{HS}$) is different from $ES7_{CA}$ in size (876 nts), composition (~80% GC content), sequence, and structure.

We demonstrate that isolated $ES7_{CA}$, like ES7 from *S. cerevisiae* ($ES7_{SC}$),[19] and $ES7_{HS}$ (Lizzette M. Gómez Ramos and Loren Dean Williams, unpublished) folds reversibly to a near-native state. We investigate the interactions of isolated $ES7_{CA}$ with aminosugars, which are known to bind to bacterial ribosomes. An assay to screen library of peptidic aminosugars (PAs) for binding to ES7 was developed. Relative affinities of PAs (Figure 1) for

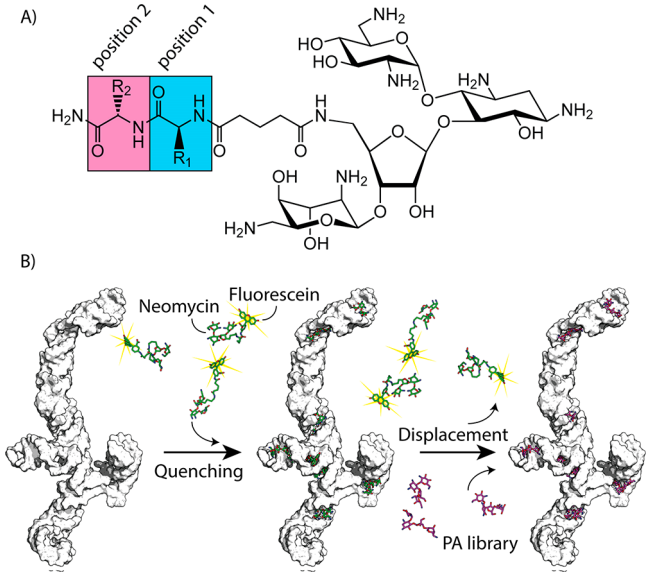

Figure 1. Affinities of a library of PAs (peptidyl amino sugars) for $ES7_{CA}$ were investigated by a fluorescence displacement assay. (A) Structures of PAs. Position 1 is blue. Position 2 is pink. R_1 and R_2 are amino acid side chains. (B) Schematic diagram of the assay showing displacement of fluorescein-neomycin (F-neo, green) by a competitive ligand (PAs, purple) from a three-dimensional model of $ES7_{CA}$. The yellow star indicates fluorescence.

$ES7_{CA}$ were assessed with fluorescence displacement assays and differential thermal melting studies. Members of the PA library with high affinity for $ES7_{CA}$ were investigated to determine the minimum inhibitory concentration (MIC) needed to induce mortality of *C. albicans*. PAs with the lowest MICs were tested for cytotoxic effects in HEK293T cells. PAs that bind with high affinity and specificity to $ES7_{CA}$ *in vitro*, in comparison to $ES7_{HS}$, induce mortality in *C. albicans* but not in HEK293T cells. Our results suggest selectivity and activity of selected PAs for specific rRNAs and species, and indicate that ESs might represent useful targets for the development of new chemotherapeutics directed against eukaryotic pathogens.

MATERIALS AND METHODS

Synthesis of $ES7_{CA}$ and $ES7_{HS}$ rRNAs. The DNA encoding $ES7_{CA}$, appended to the T7 promoter, flanked by restriction sites for *Eco*RI (5′ end) and *Hin*dIII (3′ end), was constructed by recursive PCR.[27] The DNA was ligated into restricted, dephosphorylated pUC19, and transformed into competent DH5α cells. Colonies were selected on X-gal Blue-White screening (Thermo Scientific). Oligomer and primer sequences used in the recursive PCR are shown in Tables S.1 and S.2. Oligomers, primers, and DNA sequencing were obtained from Eurofins-MWG Operon. The gene encoding $ES7_{HS}$, with the T7 promoter and restriction sites for *Eco*RI (5′ end) and *Hin*dIII (3′ end), in pUC57-Kan was purchased from Genewiz.

The SHAPE structural cassette[28] was incorporated onto the 3′ end of $ES7_{CA}$ with the Q5 Site-directed mutagenesis kit (New England BioLabs) to allow SHAPE mapping of the entire $ES7_{CA}$. Primer sequences are shown in Table S.4. $ES7_{CA}$ and $ES7_{HS}$ RNAs were transcribed using the HiScribe T7 high yield RNA synthesis kit (New England BioLabs) and purified as described previously.[19]

SHAPE Reactions. Selective 2′-hydroxyl acylation analyzed by primer extension (SHAPE) was adapted from published protocols.[28,29] SHAPE monitors local nucleotide flexibility through reactivity of 2′ oxygens to an electrophile. Experiments on $ES7_{CA}$ were performed as described previously.[19] Data were collected in 200 mM Na^+ and no Mg^{2+} to promote and analyze secondary structure.[30−32] Tertiary interactions were characterized by changes in SHAPE upon addition of Mg^{2+} ions without other changes in the experimental procedure. Na^+ only and Na^+/Mg^{2+} SHAPE data for $ES7_{CA}$ were normalized, and Na^+ reactivities were subtracted from Mg^{2+} reactivities at each nucleotide position as previously described.[33]

The effect of neomycin (Neo) was investigated by monitoring changes in SHAPE upon addition of Neo. Since the hydroxyl groups of the Neo ribose are expected to be modified by the SHAPE reagent, Neo concentration was elevated in the SHAPE reactions (10 mM). Control and Neo SHAPE data for $ES7_{CA}$ were normalized, and control SHAPE reactivities were subtracted from Neo reactivities at each nucleotide position.

Thermal Folding/Unfolding. Thermal melting of $ES7_{CA}$ RNA was monitored by absorbance at 260 nm in a thermostated Varian Cary-1E UV spectrophotometer. The melting buffer consisted of 180 mM NaCl, 20 mM Tris-HEPES (pH 8.0), and various concentrations of Neo. Melting, data reduction, and fitting were performed as described.[19,34]

Interactions of $ES7_{CA}$ with PAs. A library of 215 PAs (Figure 1), which use Neo as the scaffold,[35] was screened for binding to $ES7_{CA}$ using a fluorescence displacement assay.[36] Fluorescein-neomycin (F-neo) was used as the reporter molecule and was synthesized as described.

K_d's of Neomycin and ES7. Binding of F-neo to $ES7_{CA}$ was assayed in triplicate in binding buffer [50 mM NaCl, 0.4 mM EDTA, 10 mM HEPES (pH 7.0)]. F-neo concentration was fixed at 10 nM in each well of a 96-well plate, which was titrated with 2× serial dilutions of $ES7_{CA}$ from 1.58×10^{-8} M to 7.63×10^{-12} M. Binding of F-neo to $ES7_{HS}$ RNA was assayed at fixed F-neo (100 nM) titrated with 2× serial dilutions of $ES7_{HS}$ from 2.5×10^{-5} M to 1.22×10^{-8} M. F-neo was excited at 485 nm and monitored at 525 nm using a Genios Pro plate reader (Tecan). Fluorescence intensity decreased with increasing RNA because the interaction with RNA quenches F-neo emission.

The stoichiometry of binding of F-neo to ES7 was estimated from plots of fluorescence of F-neo versus molar ratio of $ES7_{CA}$ to F-neo. Separately from the stoichiometric calculation, K_d's were estimated from mass balance describing the relationship between bound F-neo, $[\text{F-neo}]_b$, and the total concentration of F-neo, $[\text{F-neo}]_{total}$, and the total concentration of RNA, $[\text{RNA}]_{total}$:

DOI: 10.1021/acs.biochem.7b00703
Biochemistry 2017, 56, 5288−5299

Chart 1

(((((((((((.....((((..((((.((((.((.....)).)))).....))))..))))..((((((((((((((((.(((((((.....(.((((((.....((((((.....))))))).....)
)))))).)....)))))).))))))))))).....((((...))))....)))))))).....))))))))))

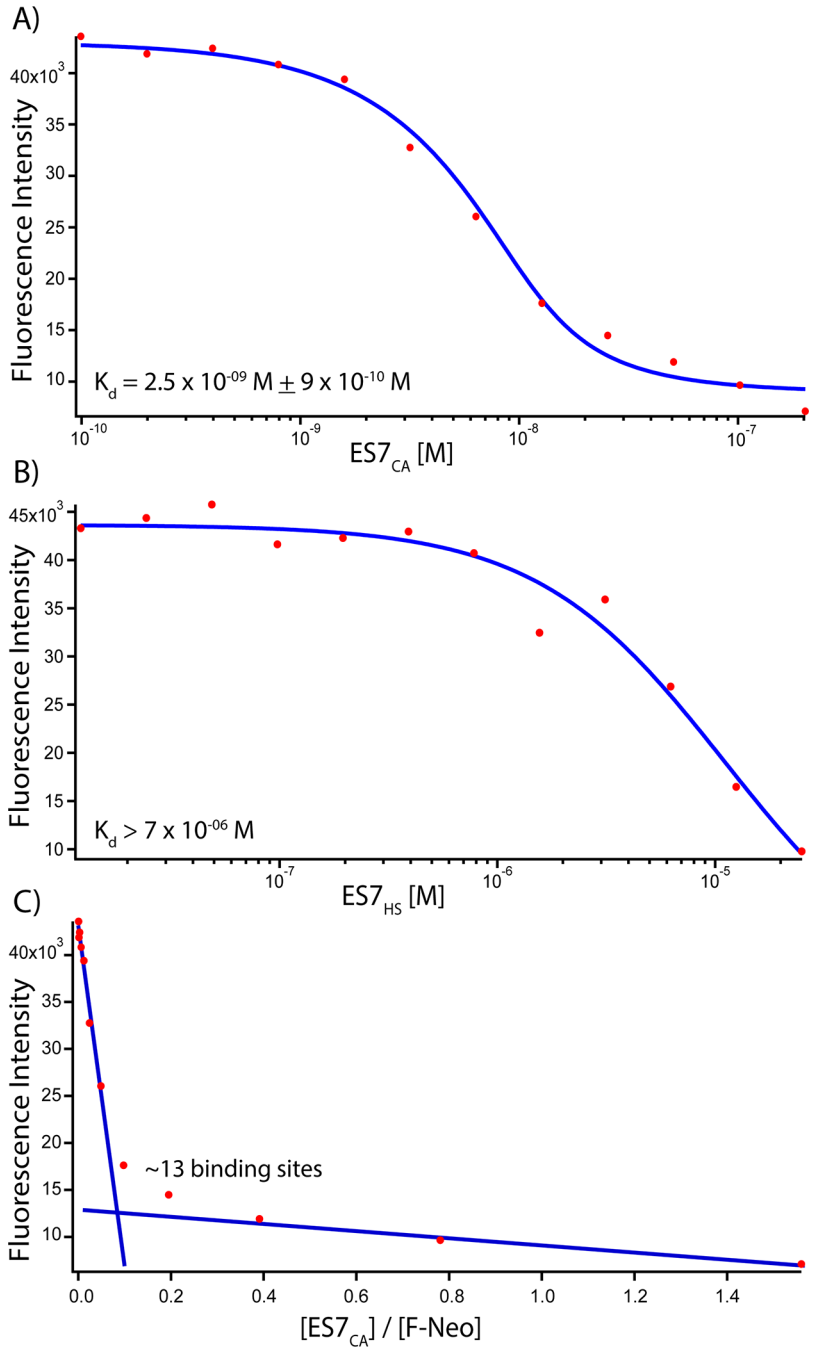

Figure 2. Binding curves of ES7 RNAs with F-neo. (A) $ES7_{CA}$ and (B) $ES7_{HS}$. The K_d of $ES7_{CA}$ and F-neo was estimated by fitting to be 2.5 nM. The K_d of $ES7_{HS}$ and F-neo was estimated to be greater than 7 μM. (C) Plot of $[ES7_{CA}]/[\text{F-neo}]$ versus fluorescence intensity. The stoichiometric coefficient of Neo in the binding reaction to $ES7_{CA}$ is estimated to be 13 from the intersection of the two lines. Titration of F-neo with $ES7_{CA}$ was performed by holding [F-neo] constant at 10 nM and increasing $[ES7_{CA}]$.

$$[\text{F-neo}]_b^2 - [\text{F-neo}]_b \times ([\text{F-neo}]_{total} + [\text{RNA}]_{total} + K_D) + [\text{F-neo}]_{total} \times \text{RNA}_{total} = 0$$

The observed emission intensity, I, is the combination of the emission from bound F-neo, I_b, and free F-neo, I_f, and is governed by a relationship that allows one to obtain $[\text{F-neo}]_b$:

$$I = I_b \times [F\text{-neo}]_b + I_f \times [\text{F-neo}]_f$$

In part because of systematic contributions to errors, actual errors may be larger than estimated errors, which assume only random contributions.

Small Molecule High Throughput Screening. High throughput screening (HTS) was performed in duplicate in

DOI: 10.1021/acs.biochem.7b00703
Biochemistry 2017, 56, 5288−5299

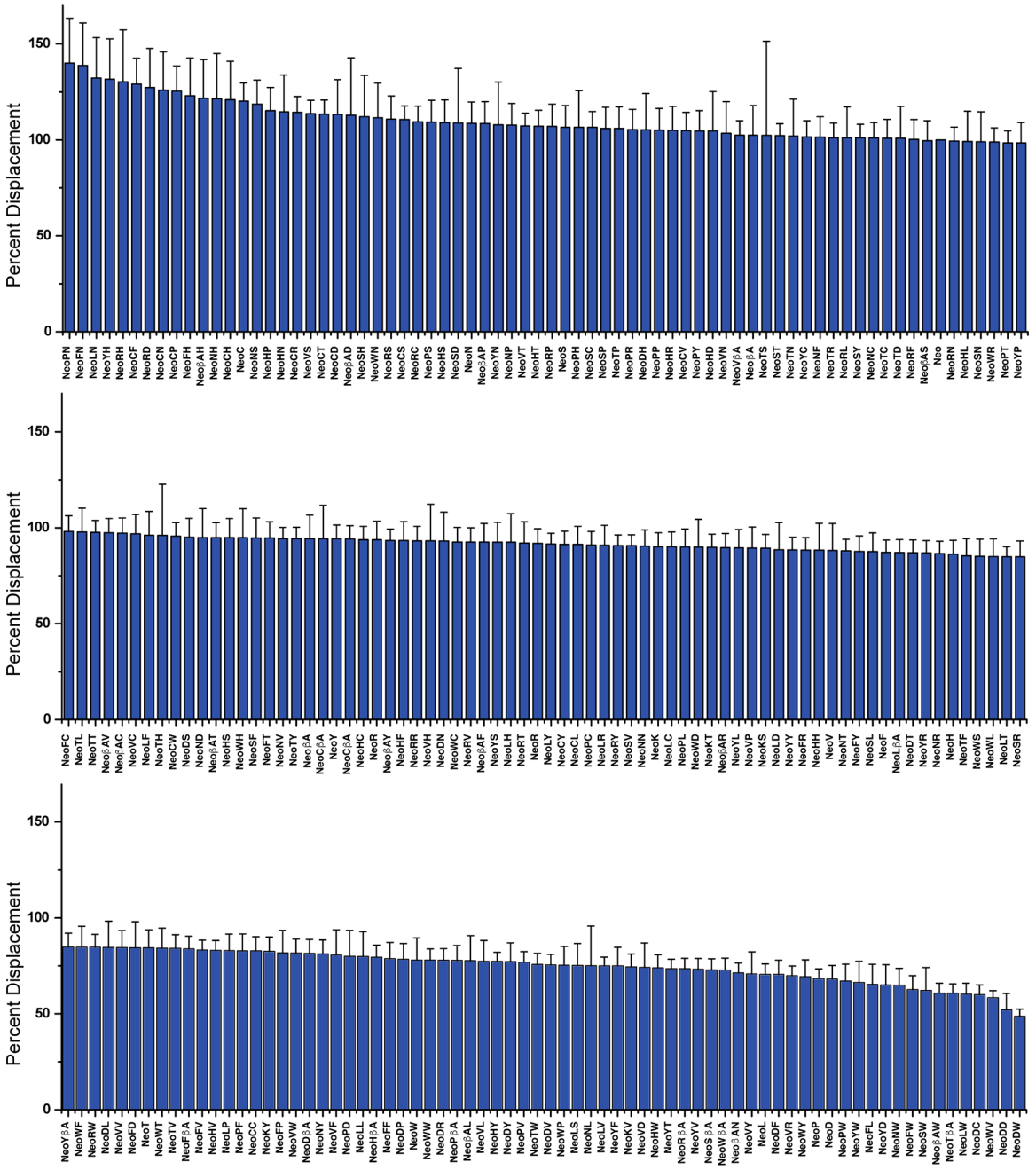

Figure 3. Ranking of 215 PAs by their tendency to displace F-neo from $ES7_{CA}$ normalized by the displacement of F-neo by Neo. Each experiment was performed in duplicate. Standard deviations are shown with error bars.

binding buffer using the fluorescence displacement assay.[36] PAs (1 μM) were added to the F-neo/ES7 mixture (100 nM F-neo and 11.6 nM ES7 RNA, final concentrations) previously aliquoted into 96-well plates. All plates contained two sets of controls, the F-neo/ES7 complex and the F-neo/ES7 complex with Neo. The displacement of F-neo by PAs was measured by the increase in fluorescence (ΔF) after addition of PAs and was compared to fluorescence of the F-neo/ES7 complex. The extent of displacement of F-neo by PAs was calculated from changes in fluorescence upon addition of PAs to the F-neo/ES7 complex (ΔF_{PA}) divided by the change in fluorescence obtained by the addition of Neo to the F-neo-ES7 complex (ΔF_{Neo}).

$$\%\text{displacement} = (\Delta F_{PA}/\Delta F_{Neo}) \times 100$$

IC_{50} Experiments. IC_{50} experiments were performed using a fluorescence displacement assay. The F-neo/ES7 complex was maintained at constant concentration (100 nM F-neo and 11.6 nM $ES7_{CA}$ RNA) and was titrated with PAs in a 96-well plate. Curve fitting was performed with Igor Pro. The IC_{50} is the inflection point of the sigmoidal fit.

Minimum Inhibitory Concentrations. Stocks of PAs were stored at 1 μM in deionized water at −80 °C. *C. albicans* SC5314 was cultured in yeast extract-peptone-dextrose (YPD) agar plates at 30 °C for 24 h. Colonies were picked and diluted in YPD media to $OD_{600} \approx 0.1$. Eighty microliters of cultivated media were aliquoted in 96-well clear flat bottom plates. Twenty microliters of diluted PA was added to each well (final concentrations of 200, 100, 50, 25, 12.5, 6.25, 3.13, 1.57, 0.78,

DOI: 10.1021/acs.biochem.7b00703
Biochemistry 2017, 56, 5288−5299

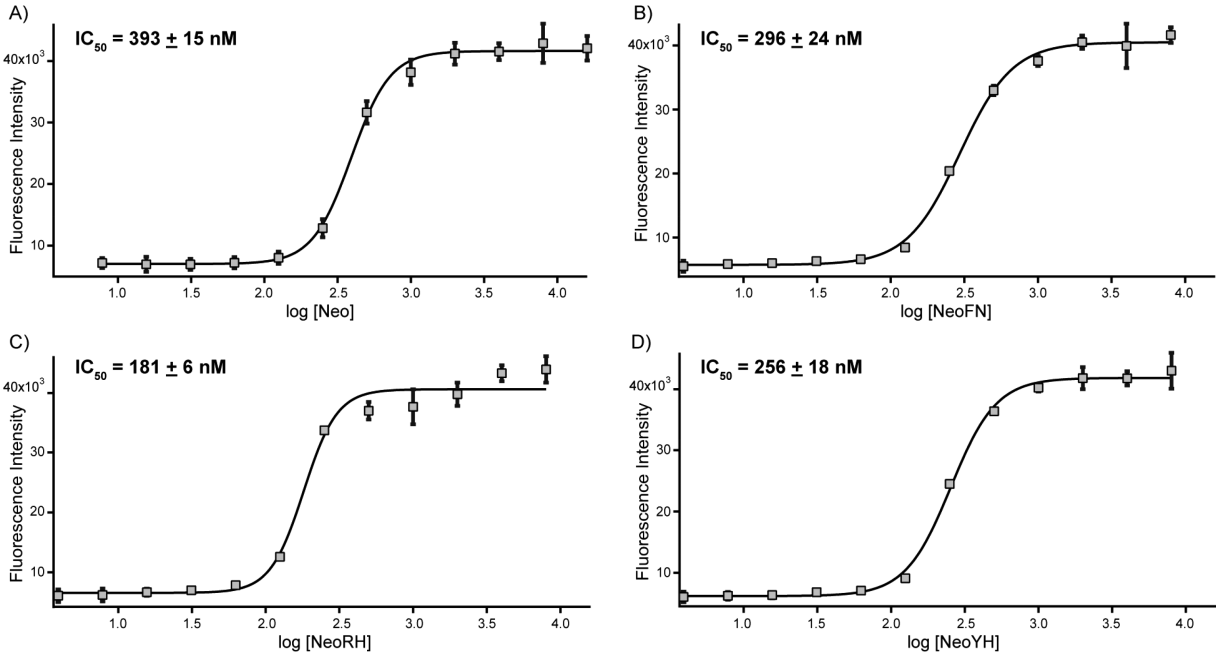

Figure 4. IC_{50} measurements of PAs. Titration of $ES7_{CA}$ was performed with (A) Neo, (B) NeoFN, (C) NeoRH, and (D) NeoYH. F-neo displacement was monitored. IC_{50} values are estimated to be Neo = 393 ± 15 nM, NeoFN = 296 ± 24 nM, NeoRH = 181 ± 6 nM, and NeoYH = 256 ± 18 nM.

0.39, 0.20, and 0.10 μM) to a final volume of 100 μL per well. Controls include 20 μL of water and 80 μL of YPD media. Standard growth was measured in 20 μL of water and 80 μL of YPD. Plates were shaken continuously at 30 °C for 24 h in a Synergy H4 Hybrid Multimode plate reader (Biotek). Absorbance at 600 nm was measured every 10 min. The effect of PA on growth was assayed by taking the absorbance at 600 nm with PA (A_{PA}) minus baseline (media alone, A_{media}), normalized by the absorbance of the standard culture (A_{ST}) minus baseline:

$$\%\text{growth} = (A_{PA} - A_{media})/(A_{ST} - A_{media}) \times 100$$

MIC values were determined after incubation of cells with PAs for 24 h.

Cytotoxicity. HEK293T cells were grown in Dulbecco's modified Eagle's medium, supplemented with 10% fetal bovine serum. Cells were incubated at 37 °C in humidified 5% CO_2. Three thousand cells were seeded in 96-well plates, with total volumes of 100 μL per well. Cell adhesion to the plates was allowed in an initial incubation period of 24 h. PAs were added to each well (100 μM final concentrations) followed by incubation for 72 h. The CellTiter 96 AQueous One Solution Cell Proliferation Assay (Promega) was used to determine cell viability. Absorbance was measured at 490 nm.

Modeling of $ES7_{CA}$. The initial secondary model of $ES7_{CA}$ was obtained by homology with the known secondary and three-dimensional structure of $ES7_{SC}$.[19,37] The $ES7_{CA}$ secondary model predicted by mFold[38] is consistent with SHAPE data. The resulting user defined secondary structure (Chart 1) was used to construct three-dimensional models using RNAComposer.[39] Three dimensional models were ranked based on energy,[40] confirmed in secondary structure with RNApdbee,[41] and used in docking studies.

RESULTS

Interactions with PAs with $ES7_{CA}$ were evaluated with SHAPE, fluorescence displacement assays, and thermal melting. Members of the PA library with greatest estimated affinities for $ES7_{CA}$ were investigated to determine MIC values in *C. albicans*. PAs with the lowest estimated MICs were tested for cytotoxicity in HEK293T cells. The secondary structure of $ES7_{CA}$ appears to be conserved when is isolated from the rest of the rRNA, as indicated by SHAPE, computational melting, and modeling.

Affinities of F-neo for $ES7_{CA}$ and $ES7_{HS}$. F-neo binds with high affinity and specificity to $ES7_{CA}$ relative to $ES7_{HS}$. The extent of binding was estimated from changes in fluorescence of F-neo during titration with RNA. The dissociation constant (K_d) for binding to $ES7_{CA}$ was estimated from nonlinear fitting of data to mass balance equations. The K_d of F-neo for $ES7_{CA}$ is estimated to be 2.5×10^{-9} M ± 9×10^{-10} M (Figure 2A). The K_d of F-neo for $ES7_{HS}$ could not be accurately determined because the affinity is lower than the practical limits of the assay >7 μM (Figure 2B). The affinity F-neo for $ES7_{CA}$ is estimated to be 2000 times greater than for $ES7_{HS}$. By contrast, K_d's for association of Neo with A site RNA, its cognate binding site, were previously estimated to be 0.053 μM for *Escherichia coli* and 0.26 μM for human.[42] This difference in A site binding (4-fold) is less than the difference in K_d of F-neo with $ES7_{CA}$ versus the K_d of F-neo with $ES7_{HS}$.

Stoichiometric coefficients were estimated by fitting the binding data of $ES7_{CA}$ to F-neo[43] (Figure 2C). Fluorescence of F-neo versus the molar ratio of $ES7_{CA}$ to F-neo is linear in the limiting regions of the binding curve. The limiting lines intersect at a molar ratio of ~0.077, suggesting a stoichiometric coefficient of F-neo of approximately 13 in the binding reaction. We assume that each binding event has the same affinity, and thus K_d implies $K_{d,apparent}$. We also assume that the stoichiometries of binding to $ES7_{CA}$ are conserved between F-neo and Neo. The binding stoichiometry for the interaction of F-neo to $ES7_{HS}$ could not be estimated due to the low affinity of F-neo for $ES7_{HS}$.

The Library. We investigated the affinities of a 215-member library of PAs (Figure 1) for $ES7_{CA}$ by several methods.[35] The library consists peptides linked by glutarate to Neo at the 5′ position of the ribose ring. Some members of the PA library are monopeptidic, with amino acids at position one only and some are dipeptidic, with amino acids at positions one and two.

DOI: 10.1021/acs.biochem.7b00703
Biochemistry 2017, 56, 5288−5299

High Throughput Screening of the PA Library for Affinity for $ES7_{CA}$. The extent of binding of PAs to $ES7_{CA}$ was estimated through HTS using a fluorescence displacement assay (Figure 2).[35,36] In this assay, $ES7_{CA}$ is first incubated with F-neo, which is then competitively displaced by a PA. The assay allows ranking of members of the PA library and is normalized so that F-neo displacement by Neo equals 100%. PAs with displacements greater than 100% bind to $ES7_{CA}$ with greater affinity than Neo. PAs with displacements less than 100% bind with less affinity than Neo. Around 60 compounds from the PA library showed greater affinity than Neo for $ES7_{CA}$ in the HTS (Figure 3). A few of these are single amino acid PAs; the others are double amino acid PAs. The low affinity of F-neo for $ES7_{HS}$ precluded estimation of the affinities of the PA library for $ES7_{HS}$.

IC_{50} Measurements of Affinity for $ES7_{CA}$. To confirm results obtained from the HTS, we performed IC_{50} measurements on several conjugates that showed F-neo displacements above the median. In the IC_{50} assay, complexes of F-neo and $ES7_{CA}$ were titrated with PAs and displacement of F-neo was monitored at various ratios of PA to $ES7_{CA}$. Binding affinities are 2.2-fold greater than Neo for NeoRH, 1.5-fold greater for NeoYH, and 1.3-fold greater for NeoFN. Thus, the IC_{50} measurements are generally consistent with the HTS results.

Minimum Inhibitory Concentrations. Inhibition of microbial growth by PAs was initially assessed through a single-dose assay. The 10 strongest binders identified in HTS (above) were tested at 200 μM for inhibition of growth of *C. albicans*. All the PAs except NeoRD and NeoPN inhibited *C. albicans* growth under these conditions.

MICs, which are more accurate measures of inhibition of growth than single dose assays, are consistent with the results obtained in the single-dose assay (Table 1). MICs for *C. albicans* were evaluated for PAs that showed activity in single dose assays. MIC is the lowest concentration of PA that inhibits *C. albicans* growth by 95% after 24 h. NeoFH, NeoRH, and NeoYH exhibited MICs of 100 μM, which are the lowest MICs obtained. NeoFN, NeoLN, NeoCN, NeoCF, and NeoCP exhibited MICs of 200 μM. NeoPN and NeoRD exhibited MICs greater than 200 μM. After 24 h at 200 μM, NeoPN and NeoRD fail to inhibit growth. Neo has a MIC of greater than 5 mM. While the MICs of the PAs evaluated here lie above the useful therapeutic range, some of them show ~50 fold improvement over Neo and provide a starting point to further modify and optimize the PAs.

Table 1. Minimal Inhibitory Concentrations (MIC)[a]

name	PA no.[b]	MIC (μM)
Neo		>5000
NeoPN	1151	>200
NeoFN	1150	200
NeoLN	1149	200
NeoYH	1182	100
NeoRH	1173	100
NeoCF	1212	200
NeoRD	1159	>200
NeoCN	1156	200
NeoCP	1226	200
NeoFH	1178	100
fluconazole		>200

[a]MIC is the concentration of PA that inhibits *C. albicans* growth by 95% at 30 °C after 24 h. Averages of triplicate experiments are reported. [b]Previously published PA numbering system.[35]

Fluconazole is a standard treatment against fungal infections. Some PAs exhibit MIC values that are superior to those of fluconazole. MICs for fluconazole determined here in a variety of experimental conditions are consistent with previous work.[44]

Cytotoxicity Assays. Useful antimicrobial agents must have target selectivity and lack of toxicity toward the host. Cytotoxicity studies suggest that PAs are not toxic to human cells (Figure 5). HEK293T cells were incubated for 72 h with Neo, NeoRH, NeoFH, and NeoYH at their MIC values of 100 μM. The results indicate a survival rate of around 70% or higher.

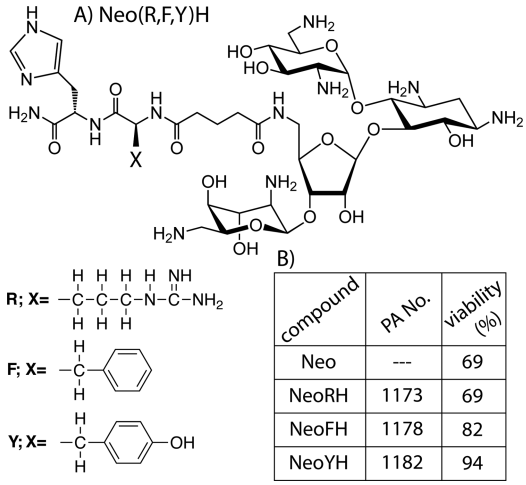

compound	PA No.	viability (%)
Neo	---	69
NeoRH	1173	69
NeoFH	1178	82
NeoYH	1182	94

Figure 5. Cytotoxicity of PAs in human cells. PAs were incubated with HEK293T cells for 72 h at 100 μM. (A) Chemical structures of NeoRH, NeoFH, and NeoYH. (B) Cell viability is reported in comparison to that of PA-free cells.

General Trends in Structure and Function. The HTS results suggest that 10 of the 20 best $ES7_{CA}$ binders in the PA library contain aromatic amino acids. The results also suggest that single amino acid conjugates that exhibit higher affinity than Neo for $ES7_{CA}$ (NeoS, NeoC, and NeoN) contain amino acids that are polar and uncharged, including serine, cysteine, and asparagine (Figure 3). An exception to this is NeoβA, which contains a nonpolar amino acid. Single amino acid conjugates, NeoD and NeoP, show the lowest affinity for $ES7_{CA}$, displacing F-neo at 68% under our experimental conditions (Figure 3). The low affinity of anionic NeoD is expected since RNA is also negatively charged.

Double amino acid conjugates with positively charged and polar amino acids, including PAs containing asparagine, histidine, or cysteine at either the first or second position, exhibit higher affinities for $ES7_{CA}$. NeoPN displays the highest affinity for $ES7_{CA}$ with 140% displacement, which is very similar to that of NeoFN, NeoLN, and NeoYH. The conjugation of two positive charges to the PAs does not seem to enhance the binding to $ES7_{CA}$ (Figure 3). Negative charge is unfavorable. Three of the 10 worst binders contain an aspartic acid in the first position. Conjugation to a tryptophan also appears detrimental for binding to $ES7_{CA}$; 7 of the 10 worst binders belong to this category. The worst binding double amino acid conjugates contain negatively charged or bulky amino acids.

IC_{50} results are generally consistent with the HTS results. IC_{50} results obtained with double amino acid conjugates confirm that binding to $ES7_{CA}$ is strengthened when the Neo scaffold is conjugated to positively charged and polar amino acids. IC_{50} results also suggest that conjugation to amino acids with smaller

DOI: 10.1021/acs.biochem.7b00703
Biochemistry 2017, 56, 5288−5299

aromatic systems and greater hydrogen bonding capabilities can improve the affinity toward $ES7_{CA}$. Of all the conjugates tested, NeoRH displays the greatest affinity. This PA contains the smallest aromatic system and the most hydrogen donors of the three PAs tested for IC_{50}.

MIC experiments suggest that the second amino acid position is important for PA activity *in vivo*. Compounds conjugated to a histidine in the second amino acid position exhibit the lowest MICs. Overall, the amino acids conjugated at this position follow a well-defined pattern; most of them are polar, with hydrogen bonding capabilities. NeoRD is an exception and exhibited higher values of MIC. Histidine is the smallest aromatic amino acid and possesses two sites for hydrogen bonding. It seems likely that a combination of geometry and hydrogen bonding capabilities at the second amino acid position offer interactions with the PA-$ES7_{CA}$. No specific contribution could be deduced for the first amino acid position, as no definite trend is observed.

Secondary Structure of $ES7_{CA}$. Isolated $ES7_{CA}$ folds to a native-like secondary structure in the presence of Na^+, with four primary helices (ES7a, ES7b, and ES7c and Helix 25, Figure 6). The secondary structure of isolated $ES7_{CA}$ was determined by SHAPE footprinting,[45,46] computational folding,[38] and secondary structure homology modeling. As shown in Figure 6A, nucleotides in helical regions are the least reactive in the SHAPE assay.

ΔMg^{2+} Heat Maps of $ES7_{CA}$. The conformation of isolated $ES7_{CA}$ changes upon addition of Mg^{2+}. SHAPE reactivity obtained in the presence of Na^+ alone (Figure 6A) was subtracted from reactivity in the presence of both Na^+ and Mg^{2+} (Figure 6B) to give a ΔMg^{2+} heat map (Figure 6C). The ΔMg^{2+} heat map identifies nucleotides that exhibit Mg^{2+}-dependence of SHAPE reactivity, which can be either positive or negative. Helical regions are invariant to Mg^{2+} (white on the ΔMg^{2+} heat map) as expected,[30,32] indicating that secondary structure forms in the presence of Na^+ alone and is maintained upon Mg^{2+} addition. Mg^{2+}-specific changes in SHAPE reactivity are focused in bulges, loops, and nonhelical regions. It seems possible that some of these nucleotides are involved in long-range interactions in the native state, which are favored by the addition of Mg^{2+}.[30,32] This work provides the first structural data on any rRNA of *C. albicans*.

Comparison of SHAPE data obtained for $ES7_{CA}$ (Figure 6) and $ES7_{SC}$[19] show that the ES7s of these fungi share similar secondary and tertiary structures. Our SHAPE data obtained previously for isolated $ES7_{SC}$ matches the predicted models of the $ES7_{SC}$ secondary structure[19] and the SHAPE reactivity of the $ES7_{SC}$ of the assembled *S. cerevisiae* ribosome.[48] ES7 for both organisms consists of four helices and a primary junction where Helices ES7a, ES7c, and 25 are joined. This junction is the region of greatest changes in SHAPE upon addition of Mg^{2+}. Many of the bulges and helical mismatches show changes in SHAPE upon addition of Mg^{2+}. The loops and mismatches are conserved between $ES7_{CA}$ and $ES7_{SC}$, as are changes in SHAPE reactivity of these regions upon Mg^{2+} addition.

ΔNeo Heat Maps of $ES7_{CA}$. SHAPE data, obtained under saturating Neo, allow characterization of ligand-induced conformational changes of RNA but do not allow determination of differential affinities of the multiple Neo binding sites. Neo binds to $ES7_{CA}$ with high stoichiometry, as indicated by binding assays (see above) and is therefore assumed to occupy multiple binding sites during the SHAPE experiments. SHAPE reactivity obtained in the presence of saturating Neo was subtracted from the SHAPE reactivity obtained in the absence of Neo to give a ΔNeo heat map (Figure 7). We have obtained ΔNeo heat maps in the presence and absence of Mg^{2+}.

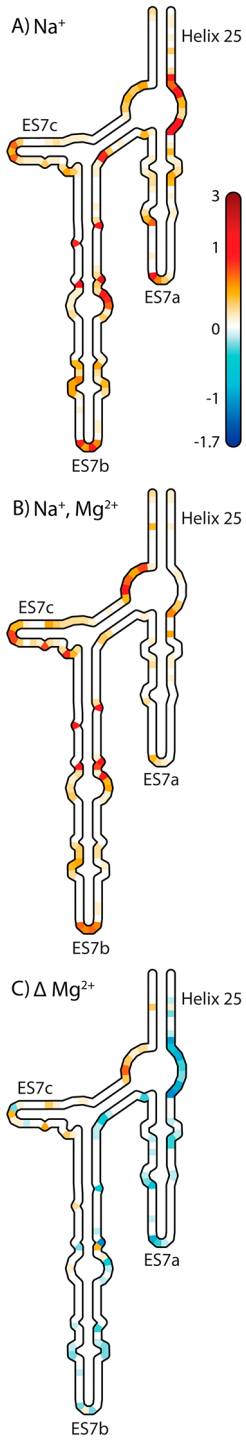

Figure 6. (A) SHAPE heat maps in the presence of Na^+ alone are consistent with the proposed secondary structural model of $ES7_{CA}$. Helical regions are unreactive (white), while loops and bulges are reactive (red). (B) Addition of Mg^{2+} does not disrupt the secondary structure. (C) A delta map (ΔMg^{2+}), showing changes in reactivity upon addition of Mg^{2+} indicate Mg^+-induced changes in the structure of $ES7_{CA}$. Nucleotides with positive values (red) indicate higher reactivity upon addition of Mg^{2+}. Nucleotides with negative values (blue) indicate decreased reactivity. All reactions contained 200 mM NaOAc, 50 mM NaHEPES (pH 8.0). Figures were generated with the program RiboVision.[47]

DOI: 10.1021/acs.biochem.7b00703
Biochemistry 2017, 56, 5288−5299

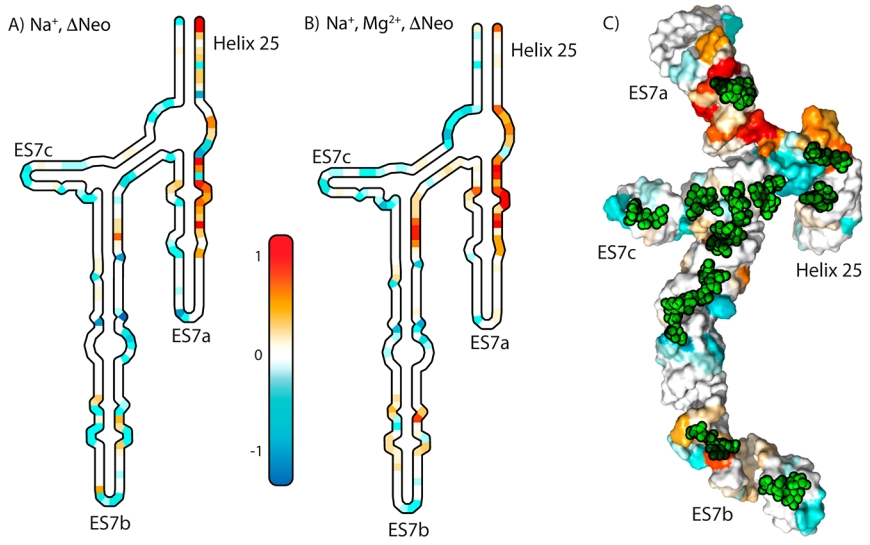

Figure 7. Δ Heat maps showing changes in SHAPE reactivity of $ES7_{CA}$. (A) Changes in reactivity upon addition of Neo in Na^+ only. (B) Changes upon addition of Neo in Na^+/Mg^{2+}. (C) Docking of Neo (green) on a three-dimensional model of $ES7_{CA}$. Δ Neo data from panel B is mapped onto a three-dimensional model of $ES7_{CA}$. Red indicates increase in reactivity. Blue indicates decrease in reactivity. Experimental conditions and methods of data analysis are the same as in Figure 6. Three dimensional figures were generated with the program PyMOL.[54]

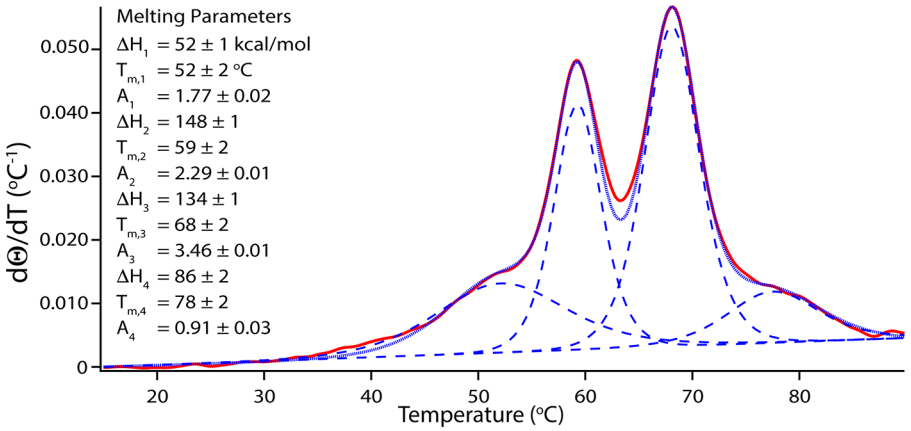

Figure 8. Melting profile of $ES7_{CA}$ rRNA, showing the derivative of the fraction unfolded with respect to temperature, monitored at 260 nm. The melting profile was fit to a nonsequential, independent transition model, with four transitions with the program Igor Pro. The enthalpy (ΔH_n), melting temperature ($T_{m,n}$), and the relative hyperchromicity (A_n) were estimated for each transition, *n*. The observed profile is red, the fit is solid blue, and the deconvolution of the fit is dashed blue.

ΔNeo heat maps in both the presence and absence of Mg^{2+} (Figure 7) show that Neo dependent-changes in reactivity are broadly distributed throughout $ES7_{CA}$. This distribution is consistent Neo-induced changes in conformation and base pairing. Nucleotides located in the main junction, helical loops, single-stranded, and mismatch regions exhibit the most intense signals in both ΔNeo heat maps. The locations of Neo-dependent changes in SHAPE reactivity are consistent with base pairing and conformational changes in regions of noncanonical secondary structure.[49−53] The induction of large scale conformational fluctuations are not inconsistent with our data. Similarities in the ΔNeo heat maps obtained in the absence and presence of Mg^{2+} shows that binding is not substantially altered by formation of tertiary structure. Mg^{2+} does not appear to compete with Neo, and it is not required for Neo binding to ES7 (Figure 7A,B).

Thermal Folding/Unfolding of $ES7_{CA}$. Isolated $ES7_{CA}$ is well-behaved in solution. As temperature changes, $ES7_{CA}$ folds and unfolds reversibly in a multistate process. The number of melting transitions of $ES7_{CA}$ were estimated, along with the T_m's and thermodynamic parameters, from nonlinear fitting of observed melting profiles to predictions of a multistate model with independent transitions (Figure 8).[34,55] Thermodynamic parameters were estimated previously for $ES7_{SC}$[19] and $ES7_{HS}$ (Lizzette M. Gomez Ramos and Loren Dean Williams, unpublished). Melting profiles are plots of the derivative of the fraction unfolded ($d\theta/dT$) versus temperature.

The unfolding profile of $ES7_{CA}$ is similar to that of $ES7_{SC}$.[19] The best fits for both these fungal ESs were obtained with four transition models. For $ES7_{CA}$ in 180 mM NaCl, the melting temperatures of the four unfolding transitions ($T_{m,n}$) are $T_{m,1}$ = 52 °C, $T_{m,2}$ = 59 °C, $T_{m,3}$ = 68 °C, and $T_{m,4}$ = 78 °C. Under the same conditions, $T_{m,1}$ is the same for $ES7_{CA}$ and $ES7_{SC}$. However, $T_{m,2}$, $T_{m,3}$, and $T_{m,4}$ for $ES7_{CA}$ are around ∼5 °C less than the corresponding T_m's of $ES7_{SC}$. The results suggest that $ES7_{CA}$ is less stable than $ES7_{SC}$. As observed for $ES7_{SC}$, the T_m's of $ES7_{CA}$ are constant with varying RNA concentrations, indicating that the transitions are unimolecular.

DOI: 10.1021/acs.biochem.7b00703
Biochemistry 2017, 56, 5288−5299

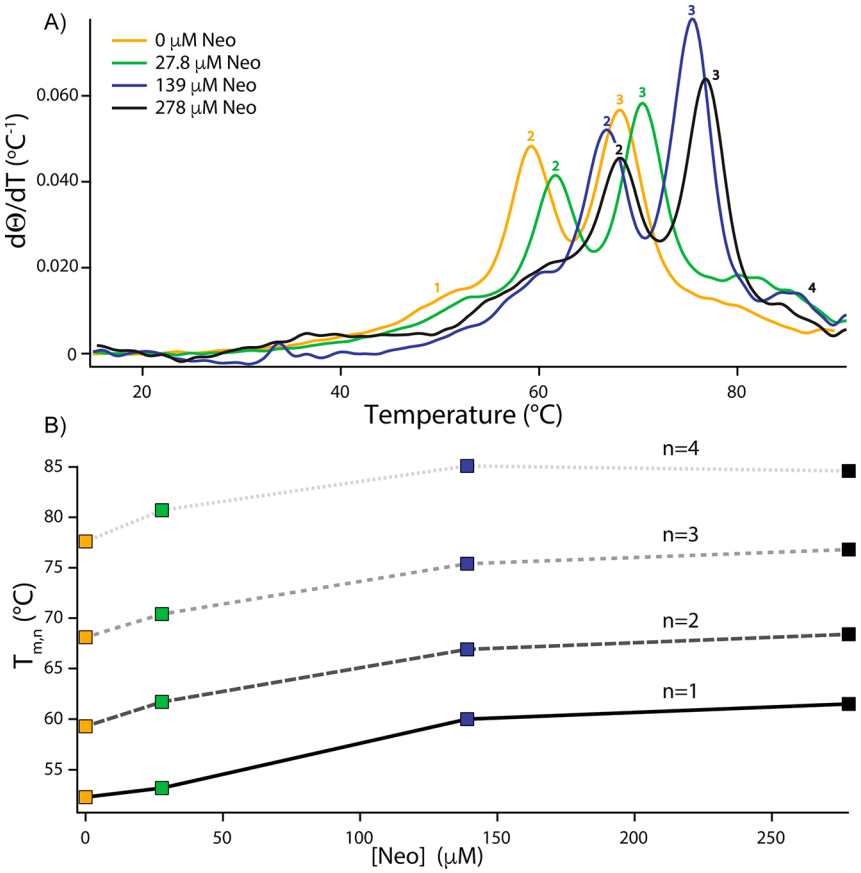

Figure 9. Melting profiles of $ES7_{CA}$ at various concentrations of Neo. (A) The derivative of the fraction unfolded with respect to temperature at 260 nm suggests four melting transitions (n = 1, 2, 3, 4). Increased [Neo] causes each $T_{m,n}$ to increase. (B) The four $T_{m,n}$ of $ES7_{CA}$ plotted versus [Neo]. The melting transition number n is indicated for each peak in both panels.

Neo stabilizes $ES7_{CA}$. Melting profiles for $ES7_{CA}$ were obtained at five molar ratios of Neo to $ES7_{CA}$ (0 μM Neo, 2.78 μM, 27.8 μM, 139 μM, and 278 μM, at constant 278 nM $ES7_{CA}$). The overall stability of $ES7_{CA}$ increases with increasing concentration of Neo as indicated by monotonic changes in all four $T_{m,n}$'s (Figure 9). The results are consistent with a model (above) in which Neo binds to $ES7_{CA}$ at broadly distributed sites, of roughly equivalent affinities. It appears that Neo binds to both native and partially unfolded intermediates. Additional information on fitting procedures and parameter estimations are provided in Supporting Information.

DISCUSSION

Translation is the most conserved[1,56−58] and highly networked[59] cellular system. Perturbations to a variety of functional sites of the ribosome can have dramatic consequences, often leading to toxicity.[4] Eukaryotic ESs are attractive drug targets because they are idiosyncratic, are located on the ribosomal surface, and are putative binding sites for a variety of proteins and cofactors. Although bacterial ribosomes are important drug targets,[60] thus far fungal ribosomes have not been explored as drug targets. Fungal ribosomes are considered poor targets in part because of acute similarities in sequence and structure between fungal and human ribosomes in the A site, P site, exit tunnel, and peptidyl transfer center regions. Instead, chemotherapeutics target fungal target cell walls, membranes, and nucleotide biosynthetic pathways.[61] The diversity of RNA functions, which are only recently being understood, suggests that small molecule binding to RNAs may provide new avenues to useful therapeutics.[62] Targets have emerged including ribozymes, riboswitches,[63] microRNAs,[64] and mRNAs.[65]

Human and fungal ribosomes are highly divergent in their ESs, and therefore fungal ESs are inviting drug targets. Our goal is to determine if ES rRNAs can be developed as useful targets for chemotherapeutics directed at eukaryotic pathogens. Fungal translation can be targeted with specificity as evidenced by the activity of Sordarins, which inhibit ribosomal translation in fungi by interacting with elongation factor 2 (EF-2).[66]

Aminoglycosides such as Neo are useful lead compounds for a discovery process for targeting fungal ribosomes. Aminoglycosides bind to rRNA and are active against Gram-positive and Gram-negative bacteria.[67] In bacteria, Neo associates with the A site decoding region of 16S rRNA, inducing changes in mRNA-tRNA conformation leading to amino acid misincorporation in the nascent protein.[68,69] Aminoglycoside-induced mistranslation is thought to promote protein misfolding and cell death.[70,71]

Here we show that Neo binds tightly and selectively to $ES7_{CA}$ *in vitro*. The K_d of F-Neo for $ES7_{CA}$ is in the low nanomolar range, similar to the K_d of Neo for the bacterial A site.[72] Neo appears to be specific for *C. albicans* ES7 over human ES7. F-Neo binds to $ES7_{CA}$ with 2000× greater K_d than to $ES7_{HS}$. $ES7_{CA}$ and $ES7_{HS}$ share low similarity in sequence, size, and structure. $ES7_{HS}$ is four-times larger than $ES7_{CA}$ with signficantly greater GC content.

HTS of a 215 member PA library (Figure 1) reveals 63 compounds that appear to bind with greater affinity than Neo to $ES7_{CA}$. This library was previously screened for antibacterial activity in Gram-negative and Gram-positive bacteria and for

DOI: 10.1021/acs.biochem.7b00703
Biochemistry 2017, 56, 5288−5299

binding to *E. coli* A site rRNA.[35] PAs in which polar and positively charged amino acids are conjugated at the second position (Figure 3) exhibit the greatest affinity for $ES7_{CA}$. NeoFH and NeoYH have lower IC_{50} values than Neo and NeoFN. MIC values were determined for the 10 best $ES7_{CA}$ binders from the HTS using *C. albicans*. NeoFH, NeoRH, and NeoYH exhibited the lowest MIC values (100 μM). Our results suggest that the geometry and hydrogen bonding capabilities of the second amino acid position are important for binding and antifungal activities. PAs with histidine at the second position exhibit the lowest IC_{50} values and MIC values.

Thermal melting, SHAPE, binding assays, and modeling suggest that $ES7_{CA}$ has multiple binding sites for Neo. Saturation plots suggest that there are ~13 binding sites for Neo in ES7. Neo is known to interact with various rRNA structures including hairpins,[49,50] internal bulges,[50] single-stranded RNA,[51] telomeric DNA,[73] DNA triple helices,[53,74−76] RNA triple helices,[52,53] and DNA−RNA hybrid helices.[52] SHAPE experiments suggest that Neo causes conformational changes to internal loops, hairpins, single-strand regions, and mismatches of $ES7_{CA}$.

The results here are consistent with a model in which $ES7_{CA}$ is a target for certain PAs. This model is supported with tight binding to $ES7_{CA}$ *in vitro* and with the MIC results. Binding of PA-compounds to $ES7_{CA}$ *in vivo* might disrupt core ribosomal function or could disturb interactions with nonribosomal proteins that are essential for cell viability.[19] In sum, ESs appear to be reasonable targets for future drug target studies and that ESs may emerge as useful new targets for antimicrobials.

It seems unlikely that Neo or PAs bind tightly to the A site of *C. albicans* rRNA, which is very similar in sequence and structure to the human A site (Figure S.4). Arya demonstrated that Neo binds with low affinity to the human A site.[35] Our cytotoxicity studies here suggest that PAs are nontoxic to human cells.

Conclusions. Isolated $ES7_{CA}$ is stable, folds autonomously, and adopts a near-native state. PAs bind with high affinity and selectivity to $ES7_{CA}$. Moreover, PAs with high affinity for $ES7_{CA}$ induce mortality on *C. albicans* but not in HEK293T cells. Additional experiments are required to confirm that the mechanism of mortality in *C. albicans* is related to binding of the lead compounds to ES7.

■ ASSOCIATED CONTENT

Supporting Information

The Supporting Information is available free of charge on the ACS Publications website at DOI: 10.1021/acs.biochem.7b00703.

Design of $ES7_{CA}$ rRNA (Table S.1-S.4), the docking of F-neo and Neo onto the three-dimensional structure of $ES7_{CA}$, the sequence alignment of ES7 rRNAs (Figure S.1), the goodness of fit for the estimation of dissociation constants (Figure S.2), the thermal melting of $ES7_{CA}$ rRNA at 260 nm (Figure S.3), the estimation of melting parameters for $ES7_{CA}$ melting (Table S.5), and the secondary structures of the A site of *E. coli*, *C. albicans* and *H. sapiens* (Figure S.4) (PDF)

■ AUTHOR INFORMATION

Corresponding Author

*E-mail: loren.williams@chemistry.gatech.edu. Phone: (404) 385-6258. Fax: (404) 894-7452.

ORCID

Liuwei Jiang: 0000-0001-6178-4505

Dev P. Arya: 0000-0001-5873-1066

Loren Dean Williams: 0000-0002-7215-4194

Funding

This work was funded by NASA (Grant No. NNX16AJ29G). D.P.A. acknowledges funding through the National Institute of Health (Grant Nos. AI114114 and R42GM097917). K.J.P. acknowledges funding through Foundation for Polish Science (Grant No. HOMING PLUS/2012-6/12). L.M.G.R. acknowledges funding through the National Science Foundation Graduate Research Fellowship (Grant No. DGE-1148903) and the Alfred P. Sloan & GaTech UCEM Minority Doctoral Fellowship.

Notes

The authors declare the following competing financial interest(s): D.P.A. has ownership interest in NUBAD, LCC.

■ ACKNOWLEDGMENTS

C. albicans was a gift from Dr. Mark P. Styczynski. The authors thank Ms. Jessica C. Bowman and Drs. Roger M. Wartell and Chad R. Bernier for discussions.

■ REFERENCES

(1) Hsiao, C., Mohan, S., Kalahar, B. K., and Williams, L. D. (2009) Peeling the onion: ribosomes are ancient molecular fossils. *Mol. Biol. Evol. 26*, 2415−2425.

(2) Melnikov, S., Ben-Shem, A., Garreau de Loubresse, N., Jenner, L., Yusupova, G., and Yusupov, M. (2012) One core, two shells: bacterial and eukaryotic ribosomes. *Nat. Struct. Mol. Biol. 19*, 560−567.

(3) Sutcliffe, J. A. (2005) Improving on nature: antibiotics that target the ribosome. *Curr. Opin. Microbiol. 8*, 534−542.

(4) Hermann, T. (2005) Drugs targeting the ribosome. *Curr. Opin. Struct. Biol. 15*, 355−366.

(5) Tenover, F. C. (2006) Mechanisms of antimicrobial resistance in bacteria. *Am. J. Med. 119*, S3−10 discussion S62−70..

(6) World Health Organization (2014) *Antimicrobial Resistance: Global Report on Surveillance*.

(7) Silver, L. L. (2011) Challenges of antibacterial discovery. *Clin. Microbiol. Rev. 24*, 71−109.

(8) McNeil, M. M., Nash, S. L., Hajjeh, R. A., Phelan, M. A., Conn, L. A., Plikaytis, B. D., and Warnock, D. W. (2001) Trends in mortality due to invasive mycotic diseases in the United States, 1980−1997. *Clin. Infect. Dis. 33*, 641−647.

(9) Ware, V. C., Tague, B. W., Clark, C. G., Gourse, R. L., Brand, R. C., and Gerbi, S. A. (1983) Sequence analysis of 28S ribosomal DNA from the amphibian Xenopus laevis. *Nucleic Acids Res. 11*, 7795−7817.

(10) Clark, C. G., Tague, B. W., Ware, V. C., and Gerbi, S. A. (1984) Xenopus laevis 28S ribosomal RNA: a secondary structure model and its evolutionary and functional implications. *Nucleic Acids Res. 12*, 6197−6220.

(11) Hassouna, N., Mithot, B., and Bachellerie, J. P. (1984) The complete nucleotide sequence of mouse 28S rRNA gene. Implications for the process of size increase of the large subunit rRNA in higher eukaryotes. *Nucleic Acids Res. 12*, 3563−3583.

(12) Gerbi, S. A. (1996) Expansion segments: Regions of variable size that interrupt the universal core secondary structure of ribosomal RNA, In *Ribosomal RNA—Structure, Evolution, Processing, and Function in Protein Synthesis* (Zimmermann, R. A., and Dahlberg, A. E., Eds.), pp 71−87, CRC Press, Boca Raton, FL.

(13) Ben-Shem, A., Jenner, L., Yusupova, G., and Yusupov, M. (2010) Crystal structure of the eukaryotic ribosome. *Science 330*, 1203−1209.

(14) Ramesh, M., and Woolford, J. L., Jr. (2016) Eukaryote-specific rRNA expansion segments function in ribosome biogenesis. *RNA 22*, 1153−1162.

(15) Jeeninga, R. E., Van Delft, Y., de Graaff-Vincent, M., Dirks-Mulder, A., Venema, J., and Raué, H. A. (1997) Variable regions V13 and

DOI: 10.1021/acs.biochem.7b00703
Biochemistry 2017, 56, 5288−5299

V3 of *Saccharomyces cerevisiae* contain structural features essential for normal biogenesis and stability of 5.8 S and 25S rRNA. *RNA 3*, 476.
(16) Gorab, E., Garcia de Lacoba, M., and Botella, L. M. (1995) Structural constraints in expansion segments from a midge 26S rDNA. *J. Mol. Evol. 41*, 1016−1021.
(17) Sweeney, R., Chen, L., and Yao, M.-C. (1994) An rRNA variable region has an evolutionarily conserved essential role despite sequence divergence. *Mol. Cell. Biol. 14*, 4203−4215.
(18) Gao, H., Ayub, M. J., Levin, M. J., and Frank, J. (2005) The structure of the 80S ribosome from Trypanosoma cruzi reveals unique rRNA components. *Proc. Natl. Acad. Sci. U. S. A. 102*, 10206−10211.
(19) Gómez Ramos, L. M., Smeekens, J. M., Kovacs, N. A., Bowman, J. C., Wartell, R. M., Wu, R., and Williams, L. D. (2016) Yeast rRNA Expansion Segments: Folding and Function. *J. Mol. Biol. 428*, 4048−4059.
(20) Nilsson, J., Sengupta, J., Gursky, R., Nissen, P., and Frank, J. (2007) Comparison of fungal 80 S ribosomes by cryo-EM reveals diversity in structure and conformation of rRNA expansion segments. *J. Mol. Biol. 369*, 429−438.
(21) Beckmann, R., Spahn, C. M., Eswar, N., Helmers, J., Penczek, P. a., Sali, a., Frank, J., and Blobel, G. (2001) Architecture of the protein-conducting channel associated with the translating 80S ribosome. *Cell 107*, 361−372.
(22) Nucci, M., and Marr, K. A. (2005) Emerging fungal diseases. *Clin. Infect. Dis. 41*, 521−526.
(23) Menzin, J., Meyers, J. L., Friedman, M., Perfect, J. R., Langston, A. A., Danna, R. P., and Papadopoulos, G. (2009) Mortality, length of hospitalization, and costs associated with invasive fungal infections in high-risk patients. *Am. J. Health-Syst. Pharm. 66*, 1711−1717.
(24) Edmond, M. B., Wallace, S. E., McClish, D. K., Pfaller, M. A., Jones, R. N., and Wenzel, R. P. (1999) Nosocomial bloodstream infections in United States hospitals: a three-year analysis. *Clin. Infect. Dis. 29*, 239−244.
(25) Rex, J. H., Rinaldi, M. G., and Pfaller, M. A. (1995) Resistance of Candida species to fluconazole. *Antimicrob. Agents Chemother. 39*, 1−8.
(26) Center for Disease Control and Prevention (2013) *Antibiotic Resistance Threats in the United States*.
(27) Bowman, J. C., Azizi, B., Lenz, T. K., Roy, P., and Williams, L. D. (2013) Preparation of long templates for RNA in vitro transcription by recursive PCR. *Methods Mol. Biol. 941*, 19−41.
(28) Wilkinson, K. A., Merino, E. J., and Weeks, K. M. (2006) Selective 2′-hydroxyl acylation analyzed by primer extension (SHAPE): quantitative RNA structure analysis at single nucleotide resolution. *Nat. Protoc. 1*, 1610−1616.
(29) Hsiao, C., Lenz, T. K., Peters, J. K., Fang, P. Y., Schneider, D. M., Anderson, E. J., Preeprem, T., Bowman, J. C., O'Neill, E. B., Lie, L., Athavale, S. S., Gossett, J. J., Trippe, C., Murray, J., Petrov, A. S., Wartell, R. M., Harvey, S. C., Hud, N. V., and Williams, L. D. (2013) Molecular paleontology: a biochemical model of the ancestral ribosome. *Nucleic Acids Res. 41*, 3373−3385.
(30) Brion, P., and Westhof, E. (1997) Hierarchy and dynamics of RNA folding. *Annu. Rev. Biophys. Biomol. Struct. 26*, 113−137.
(31) Colmenarejo, G., and Tinoco, I. (1999) Structure and thermodynamics of metal binding in the P5 helix of a group I intron ribozyme. *J. Mol. Biol. 290*, 119−135.
(32) Bowman, J. C., Lenz, T. K., Hud, N. V., and Williams, L. D. (2012) Cations in charge: magnesium ions in RNA folding and catalysis. *Curr. Opin. Struct. Biol. 22*, 262−272.
(33) Gulen, B., Petrov, A. S., Okafor, C. D., Vander Wood, D., O'Neill, E. B., Hud, N. V., and Williams, L. D. (2016) Ribosomal small subunit domains radiate from a central core. *Sci. Rep. 6*, 20885.
(34) Lanier, K. A., Athavale, S. S., Petrov, A. S., Wartell, R., and Williams, L. D. (2016) Imprint of Ancient Evolution on rRNA Folding. *Biochemistry 55*, 4603−4613.
(35) Jiang, L., Watkins, D., Jin, Y., Gong, C., King, A., Washington, A. Z., Green, K. D., Garneau-Tsodikova, S., Oyelere, A. K., and Arya, D. P. (2015) Rapid synthesis, RNA binding, and antibacterial screening of a peptidic-aminosugar (PA) library. *ACS Chem. Biol. 10*, 1278−1289.
(36) Watkins, D., Norris, F., Kumar, S., and Arya, D. P. (2013) A fluorescence-based screen for ribosome binding antibiotics. *Anal. Biochem. 434*, 300−307.
(37) Jenner, L., Melnikov, S., de Loubresse, N. G., Ben-Shem, A., Iskakova, M., Urzhumtsev, A., Meskauskas, A., Dinman, J., Yusupova, G., and Yusupov, M. (2012) Crystal structure of the 80S yeast ribosome. *Curr. Opin. Struct. Biol. 22*, 759−767.
(38) Zuker, M. (2003) Mfold web server for nucleic acid folding and hybridization prediction. *Nucleic Acids Res. 31*, 3406−3415.
(39) Popenda, M., Szachniuk, M., Antczak, M., Purzycka, K. J., Lukasiak, P., Bartol, N., Blazewicz, J., and Adamiak, R. W. (2012) Automated 3D structure composition for large RNAs. *Nucleic Acids Res. 40*, e112.
(40) Biesiada, M., Purzycka, K. J., Szachniuk, M., Blazewicz, J., and Adamiak, R. W. (2016) Automated RNA 3D Structure Prediction with RNAComposer. *Methods Mol. Biol. 1490*, 199−215.
(41) Antczak, M., Zok, T., Popenda, M., Lukasiak, P., Adamiak, R. W., Blazewicz, J., and Szachniuk, M. (2014) RNApdbee–a webserver to derive secondary structures from pdb files of knotted and unknotted RNAs. *Nucleic Acids Res. 42*, W368−372.
(42) Ryu, D. H., and Rando, R. R. (2001) Aminoglycoside binding to human and bacterial A-Site rRNA decoding region constructs. *Bioorg. Med. Chem. 9*, 2601−2608.
(43) Kumar, S., Kellish, P., Robinson, W. E., Jr., Wang, D., Appella, D. H., and Arya, D. P. (2012) Click dimers to target HIV TAR RNA conformation. *Biochemistry 51*, 2331−2347.
(44) Vasicek, E. M., Berkow, E. L., Bruno, V. M., Mitchell, A. P., Wiederhold, N. P., Barker, K. S., and Rogers, P. D. (2014) Disruption of the transcriptional regulator Cas5 results in enhanced killing of Candida albicans by Fluconazole. *Antimicrob. Agents Chemother. 58*, 6807−6818.
(45) Weeks, K. M., and Mauger, D. M. (2011) Exploring RNA Structural Codes with SHAPE Chemistry. *Acc. Chem. Res. 44*, 1280−1291.
(46) Wilkinson, K. A., Vasa, S. M., Deigan, K. E., Mortimer, S. A., Giddings, M. C., and Weeks, K. M. (2009) Influence of nucleotide identity on ribose 2′-hydroxyl reactivity in RNA. *RNA 15*, 1314−1321.
(47) Bernier, C., Petrov, A. S., Waterbury, C., Jett, J., Li, F., Freil, L. E., Xiong, b., Wang, L., Migliozzi, B. L. R., Hershkovits, E., Grover, M., Xue, Y., Hsiao, C., Bowman, J. C., Harvey, S. C., Wartell, J. Z., and Williams, L. D. (2014) RiboVision: Visualization and Analysis of Ribosomes. *Faraday Discuss. 169*, 195−207.
(48) Leshin, J. A., Heselpoth, R., Belew, A. T., and Dinman, J. D. (2011) High throughput structural analysis of yeast ribosomes using hSHAPE. *RNA Biol. 8*, 478−487.
(49) Famulok, M., and Huttenhofer, A. (1996) In vitro selection analysis of neomycin binding RNAs with a mutagenized pool of variants of the 16S rRNA decoding region. *Biochemistry 35*, 4265−4270.
(50) Wallis, M. G., von Ahsen, U., Schroeder, R., and Famulok, M. (1995) A novel RNA motif for neomycin recognition. *Chem. Biol. 2*, 543−552.
(51) Xi, H., Gray, D., Kumar, S., and Arya, D. P. (2009) Molecular recognition of single-stranded RNA: neomycin binding to poly(A). *FEBS Lett. 583*, 2269−2275.
(52) Arya, D. P., Coffee, R. L., Jr., and Charles, I. (2001) Neomycin-induced hybrid triplex formation. *J. Am. Chem. Soc. 123*, 11093−11094.
(53) Xue, L., Charles, I., and Arya, D. P. (2002) Pyrene-neomycin conjugate: dual recognition of a DNA triple helix. *Chem. Commun. (Cambridge, U. K.)*, 70−71.
(54) *The PyMOL Molecular Graphics System*, Version 1.8, Schrodinger, LLC.
(55) Draper, D. E., Bukhman, Y. V., and Gluick, T. C. (2001) Thermal methods for the analysis of RNA folding pathways, in *Curr. Protoc. Nucleic. Acid Chem.* 2008/04/23 ed., pp 11.13.11−11.13.13, John Wiley & Sons, Inc..
(56) Charlebois, R. L., and Doolittle, W. F. (2004) Computing prokaryotic gene ubiquity: rescuing the core from extinction. *Genome Res. 14*, 2469−2477.
(57) Koonin, E. V. (2003) Comparative genomics, minimal gene-sets and the last universal common ancestor. *Nat. Rev. Microbiol. 1*, 127−136.

DOI: 10.1021/acs.biochem.7b00703
Biochemistry 2017, 56, 5288−5299

(58) Harris, J. K., Kelley, S. T., Spiegelman, G. B., and Pace, N. R. (2003) The genetic core of the universal ancestor. *Genome Res. 13*, 407−412.
(59) Butland, G., Peregrin-Alvarez, J. M., Li, J., Yang, W., Yang, X., Canadien, V., Starostine, A., Richards, D., Beattie, B., Krogan, N., Davey, M., Parkinson, J., Greenblatt, J., and Emili, A. (2005) Interaction network containing conserved and essential protein complexes in Escherichia coli. *Nature 433*, 531−537.
(60) Wilson, D. N. (2013) Ribosome-targeting antibiotics and mechanisms of bacterial resistance. *Nat. Rev. Microbiol. 12*, 35−48.
(61) Ren, B., Huang, P., Zhang, J., He, W., Han, J., Liu, X., and Zhang, L. (2015) Main Applications of Antibiotics, In *Antibiotics: Current Innovations and Future Trends* (Sanchez, S., and Demain, A. L., Eds.), pp 19−47, Caister Academic Press, Poole, UK.
(62) Thomas, J. R., and Hergenrother, P. J. (2008) Targeting RNA with small molecules. *Chem. Rev. 108*, 1171−1224.
(63) Howe, J. A., Wang, H., Fischmann, T. O., Balibar, C. J., Xiao, L., Galgoci, A. M., Malinverni, J. C., Mayhood, T., Villafania, A., Nahvi, A., et al. (2015) Selective small-molecule inhibition of an RNA structural element. *Nature 526*, 672−675.
(64) Shortridge, M. D., and Varani, G. (2015) Structure based approaches for targeting non-coding RNAs with small molecules. *Curr. Opin. Struct. Biol. 30*, 79−88.
(65) Lee, M.-K., Bottini, A., Kim, M., Bardaro, M. F., Zhang, Z., Pellecchia, M., Choi, B.-S., and Varani, G. (2014) A novel small-molecule binds to the influenza A virus RNA promoter and inhibits viral replication. *Chem. Commun. 50*, 368−370.
(66) Dominguez, J. M., Kelly, V. A., Kinsman, O. S., Marriott, M. S., Gomez de las Heras, F., and Martin, J. J. (1998) Sordarins: A new class of antifungals with selective inhibition of the protein synthesis elongation cycle in yeasts. *Antimicrob. Agents Chemother. 42*, 2274−2278.
(67) Davies, J., and Wright, G. D. (1997) Bacterial resistance to aminoglycoside antibiotics. *Trends Microbiol. 5*, 234−240.
(68) Fourmy, D., Recht, M. I., and Puglisi, J. D. (1998) Binding of neomycin-class aminoglycoside antibiotics to the A-site of 16S rRNA. *J. Mol. Biol. 277*, 347−362.
(69) Kohanski, M. A., Dwyer, D. J., and Collins, J. J. (2010) How antibiotics kill bacteria: from targets to networks. *Nat. Rev. Microbiol. 8*, 423−435.
(70) Kohanski, M. A., Dwyer, D. J., Wierzbowski, J., Cottarel, G., and Collins, J. J. (2008) Mistranslation of membrane proteins and two-component system activation trigger antibiotic-mediated cell death. *Cell 135*, 679−690.
(71) Liu, Y., and Imlay, J. A. (2013) Cell death from antibiotics without the involvement of reactive oxygen species. *Science 339*, 1210−1213.
(72) Kaul, M., and Pilch, D. S. (2002) Thermodynamics of aminoglycoside-rRNA recognition: the binding of neomycin-class aminoglycosides to the A site of 16S rRNA. *Biochemistry 41*, 7695−7706.
(73) Ranjan, N., Andreasen, K. F., Kumar, S., Hyde-Volpe, D., and Arya, D. P. (2010) Aminoglycoside binding to Oxytricha nova telomeric DNA. *Biochemistry 49*, 9891−9903.
(74) Arya, D. P., and Coffee, R. L., Jr. (2000) DNA triple helix stabilization by aminoglycoside antibiotics. *Bioorg. Med. Chem. Lett. 10*, 1897−1899.
(75) Arya, D. P., Coffee, R. L., Jr., Willis, B., and Abramovitch, A. I. (2001) Aminoglycoside-nucleic acid interactions: remarkable stabilization of DNA and RNA triple helices by neomycin. *J. Am. Chem. Soc. 123*, 5385−5395.
(76) Arya, D. P., Micovic, L., Charles, I., Coffee, R. L., Jr., Willis, B., and Xue, L. (2003) Neomycin binding to Watson-Hoogsteen (W-H) DNA triplex groove: a model. *J. Am. Chem. Soc. 125*, 3733−3744.

DOI: 10.1021/acs.biochem.7b00703
Biochemistry 2017, 56, 5288−5299